Vibration dynamics in non-linear dual mass flywheels for heavy-duty trucks

N.B. When citing this work, cite the original published paper.

(article starts on next page)

Proceedings of

ISMA2018

International Conference on
Noise and Vibration Engineering

USD2018

International Conference on
Uncertainty in Structural Dynamics

Vibration dynamics in non-linear dual mass flywheels for heavy-duty trucks

L. Wramner [1,2]**, V. Berbyuk** [1]**, H. Johansson** [1]

[1] Chalmers University of Technology, Department of Mechanics and Maritime Sciences,
SE-412 96 Göteborg, Sweden
e-mail: **lina.wramner@chalmers.se**

[2] AB Volvo, Group Trucks Technology

Abstract

A non-linear model for simulations of a dual mass flywheel (DMF) for heavy-duty applications is proposed. The model includes internal clearances and friction. LuGre friction model is used, which depends on normal force, relative velocity between the two surfaces and an internal deflection variable. Measurements on the DMF are performed in a test rig and the test rig properties are analysed. The correlation shows that the general behaviour of the DMF is reproduced by the proposed simulation model. The viscous part of the friction is dominant for the analysed cases with zero mean torque, and a conventional Coulomb friction model would not suffice for this application. Near resonances, the model also shows a high sensitivity to internal clearances and spring stiffness. This indicates that correlation could be improved further if the static stiffness was measured with good accuracy for the relevant range of deflection angles.

1   Background

The increasing demand for higher efficiency in engines currently drives development towards down-sized and down-speeded engines and higher cylinder pressure. This leads to increased torsional vibrations and as a consequence puts higher demands on the driveline vibration damping capabilities.

Dual mass flywheels (DMFs) have the past decades proved their ability to significantly reduce torsional vibrations in passenger cars. In heavy-duty commercial vehicles conventional flywheels are still standard though and there is a need to better understand the potentials of DMFs for such applications. This work focuses on simulations of DMFs in heavy-duty applications, with the goal to accurately predict torsional vibrations in powertrains with DMFs for the complete operating speed and torque range.

A DMF consists of two flywheels torsionally connected by a series of springs at a radius. By exchanging a conventional flywheel for a DMF, the torsional resonance frequencies in the powertrain are affected in an advantageous way, leading to less excitation in the operating speed interval.

The most common way to connect the two flywheels is by means of curved springs, so called arc springs, located in a channel in the primary flywheel. Modelling and simulation approaches for this type of DMF for passenger cars have been studied before. In [1], [7], [5] and [3] the arc springs are modelled as several lumped masses connected by massless springs and with Coulomb friction introduced between these masses and the primary flywheel. In [4] a lumped mass model of the arc spring is combined with a LuGre friction model. The LuGre friction depends on the normal force, the relative velocity between the two contact surfaces and an internal deflection variable.

An alternative way to design the DMF is to instead of arc springs have several straight shorter springs connected by sliding shoes. This type of DMF exists for heavy-duty applications with engine torques up to

3500 Nm. No previous work regarding simulations for this type of DMF has been found. Although similar modelling as for the arc springs can be used, there is a need to build experience regarding realistic parameter values and to investigate the validity of the models for operating points valid for heavy-duty applications. In this paper a model for this type of DMF is proposed and evaluated.

2   The DMF

The analysed DMF has an outer diameter of about 490 mm to fit in an industry-standard SAE1 engine-gearbox interface. It is composed of a primary flywheel and a secondary flywheel torsionally connected by three parallel spring sets. Each spring set consists of two sliding shoes and two spring caps connected by three spring packages in series. This is illustrated in figure 1.
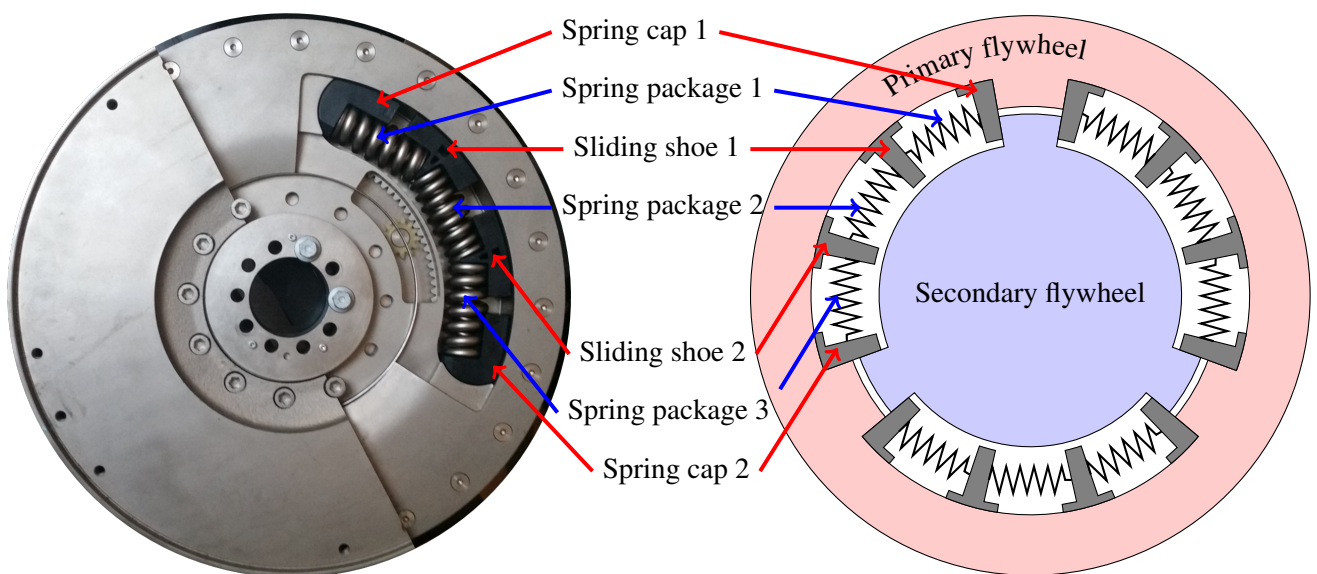

Figure 1: DMF design

The spring packages consist of two or three springs located inside each other and with slightly different lengths. The spring sets are located in a channel in the primary flywheel, with friction occurring at the contact surfaces between the primary flywheel and the sliding shoes and spring caps. When the spring packages are compressed and decompressed, the sliding shoes and spring caps slide against the primary flywheel. This results in friction forces. The normal forces at the contact surfaces depend on the compression of the springs and the centrifugal action. There is grease between the sliding shoes and the primary flywheel, and the resulting coefficient of friction will depend on the properties of the grease. These properties are generally very temperature dependent. All this means that the properties of the DMF are highly non-linear and detailed models are needed in order to accurately simulate the DMF.

2.1   Engineering model

In figure 2, the proposed torsional engineering model for the DMF in study is shown. The mass moment of inertia j_p corresponds to the primary flywheel and j_s to the secondary flywheel. It is assumed that all three spring sets are equivalent and they are modelled as one spring set represented by moments of inertia j_1 to j_4. Each spring cap can be in contact with either the primary or the secondary flywheel. For spring cap 1 this is modelled as gap activated springs with impact stiffness b_1 and gap angles θ_{1p} and θ_{1s} to primary and secondary flywheel respectively. For spring cap 2 the modelling is similar, with impact stiffness b_5 and gap
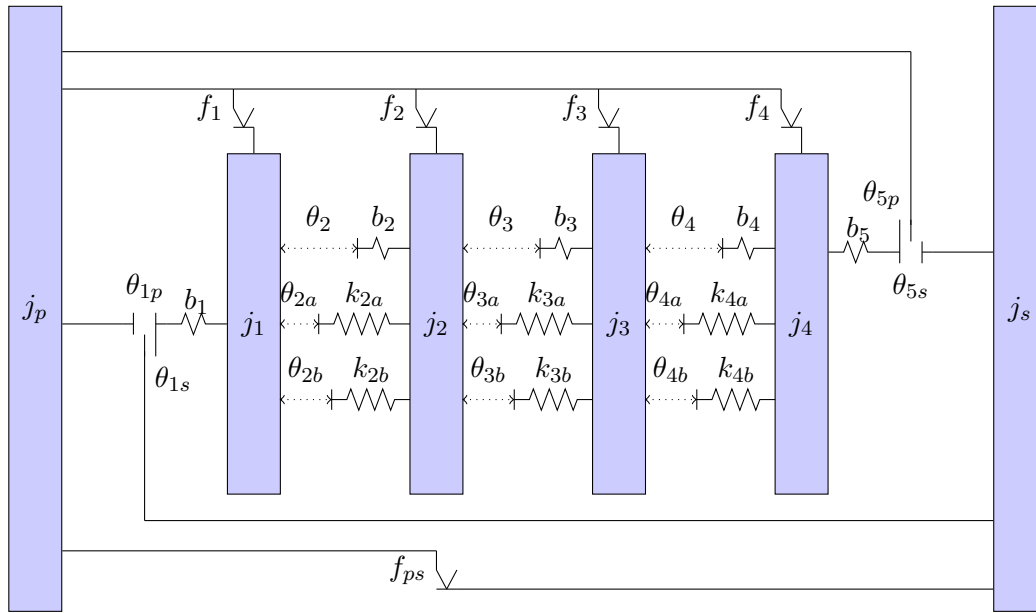
Figure 2: Engineering model of the DMF

Table 1: DMF model data

Moments of inertia	Gap angles	Stiffness
$j_p = 1.8000$ kgm^2	$\theta_{1p} = 0$ rad	$b_1 = 3.00e9$ Nm/rad
	$\theta_{1s} = 0$ rad	
$j_1 = 0.0297$ kgm^2	$\theta_{2a} = 0$ rad	$k_{2a} = 2.10e4$ Nm/rad
	$\theta_{2b} = 0.0070$ rad	$k_{2b} = 5.35e4$ Nm/rad
$j_2 = 0.0426$ kgm^2	$\theta_{3a} = 0$ rad	$k_{3a} = 1.02e4$ Nm/rad
	$\theta_{3b} = 0.0030$ rad	$k_{3b} = 5.26e3$ Nm/rad
$j_3 = 0.0426$ kgm^2	$\theta_{4a} = 0$ rad	$k_{4a} = 2.10e4$ Nm/rad
	$\theta_{4b} = 0.0070$ rad	$k_{4b} = 5.35e4$ Nm/rad
$j_4 = 0.0297$ kgm^2	$\theta_{5s} = 0$ rad	$b_5 = 3.00e9$ Nm/rad
	$\theta_{5p} = 0$ rad	
$j_s = 0.9000$ kgm^2		

angles θ_{5p} and θ_{5s}. If cases with low average torque are to be analysed, it is important to model the individual springs in each spring package separately. This is because the small differences in lengths of the different springs result in a non-linear stiffness which will influence the resonance behaviour. Spring package 1 is represented by springs k_{2a} and k_{2b}, spring package 2 by springs k_{3a} and k_{3b} and spring package 3 by springs k_{4a} and k_{4b}. Table 1 shows the data used. The torque in the measurements is not large enough for the spring caps and sliding shoes to be in contact, so the angular gaps between spring caps and sliding shoes, θ_2, θ_3, and θ_4 and the corresponding impact stiffnesses b_2, b_3 and b_4 will not affect the simulation results presented in this paper.

The friction torques at the contact surfaces between the spring caps and sliding shoes to the primary flywheel are represented by f_1 to f_4. The friction between the primary and secondary flywheel is represented by f_{ps}. The main part of this friction is believed to occur in the bearings between the two flywheels.

2.2 Friction

The geometry of the tangential connection between the flywheels and the spring caps is such that it will also take up much of the radial force. It will therefore be assumed that the friction between the spring caps and the primary flywheel will be only viscous. The friction between the sliding shoes and the primary flywheel will be modelled with the LuGre friction model. This model is described and evaluated in [6]. The friction force F depends on the relative velocity v between two surfaces, a deflection variable z and the normal force, F_n, at the interface. Equations (1) describe the standard parametrisation of the model used in this work.

$$F = \sigma_0 z + \sigma_1 \dot{z} + \sigma_2 v$$
$$\dot{z} = v - \sigma_0 \frac{|v|}{g(v)} z$$
$$g(v) = F_c + (F_s - F_c) e^{-\left(\frac{v}{v_S}\right)^2}$$

(1)

The Coulomb friction force F_c at each contact is a function of the corresponding normal force F_n and given as $F_c = \mu_c F_n$. The normal force depends on spring compressions, the angles between the sliding shoes and spring caps, the radial position of the springs and on the centrifugal action. The static friction force F_s is calculated as $F_s = \min(\mu_s F_n, F_t)$, where F_t is the total tangential force at the friction surface. In table 2, the used friction parameters are shown. The parameters are presented for one spring set and for translational direction. The friction between the primary and secondary flywheel f_{ps} is estimated as viscous damping coefficient of 5 Nms/rad. The static and kinetic friction coefficients are the same, since parameter studies have shown no significant influence of the static coefficient of friction for the analysed load cases. For higher mean torques and higher rotational speeds, the influence is expected to be higher.

Table 2: Friction parameters

Parameter	Description
$\sigma_0 = 10^5$ N/m	stiffness parameter
$v_s = 0.01$ m/s	Stribeck velocity
$\sigma_1 = 350$ Ns/m	velocity dependent damping coefficient
$\sigma_2 = 120$ Ns/m	viscous damping coefficient
$\mu_c = 0.08$	kinetic coefficient of friction
$\mu_s = 0.08$	static coefficient of friction
$r = 0.166$ m	radial position of springs
$r_f = 0.191$ m	friction contact radius
$\alpha_{2,3,4} = 0.547$ rad	angle between sliding shoes and between sliding shoes and spring caps

3 Measurements

Measurements have been performed in order to study the properties of the DMF and to enable validation of the simulated results. A rig was used that consisted of a large flywheel connected to a propeller shaft, which had a universal joint set at an angle. For a constant input angular speed, the universal joint creates an oscillating speed with oscillation frequency twice that of the input speed. The angular velocity of the rig flywheel was accelerated and then kept at a constant speed by means of a belt connected to an electric motor. The DMF was connected to the other side of the propeller shaft with some adapters and a torque meter in between as shown in figure 3. Measurements were performed for propeller shaft angles ranging
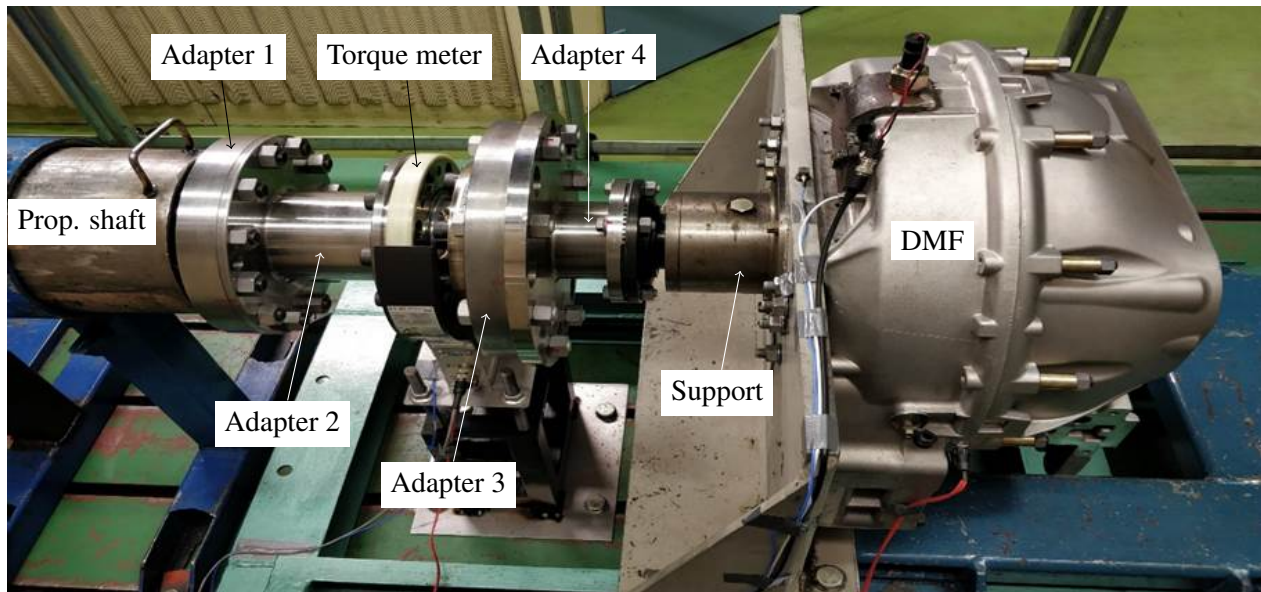
Figure 3: Rig

between 3 and 15 degrees and rotational speeds up to 1200 revolutions per minute (rpm). Angular velocities were measured at the rig flywheel and at the primary flywheel of the DMF with magnetic pickups, detecting motion of gear wheels connected to the flywheels. The number of gear teeth was 60 on the rig flywheel and 153 on the primary flywheel of the DMF. The angular velocity of the secondary DMF flywheel was measured using an optic sensor and a zebra tape with 60 black and white fields glued to the flywheel.

The friction between the sliding shoes and the primary flywheel depends on the properties of the grease. Since these properties are believed to be very temperature dependent it was considered important to measure and control the temperature. Initially, the DMF was heated until a temperature of 80 °C was obtained at the DMF surface. The temperature inside the flywheel at a distance of about 3 mm from the contact surface between the sliding shoes and the primary flywheel was recorded during the measurements. These temperatures were very stable during all measurements with values around 55 °C. The repeatability of the results was evaluated by measuring at 700 rpm both at the beginning of the measurements for a specific joint angle and after measurement had been done for all speeds under evaluation. No big deviations between the 700 rpm measurements could be seen which indicates that there were no huge differences in friction properties between the measurements. More information regarding the test procedure can be found in [2].

Table 3: Rig model structural parameters

Part	Stiffness / [Nms/rad]	Moment of inertia / [kgm^2]	label
Rig flywheel		40.0000	rig
Half propeller shaft		0.0640	joint
Propeller shaft	356000		prop
Half propeller shaft		0.0640	
Adapter 1		0.1800	
Adapter 2		0.1100	
Half torque meter		0.0485	
Bolts		0.0629	
		Total: 0.4654	
Torque meter+adapter	5997256		tm
Half torque meter		0.0485	
Adapter 3		0.3700	
Adapter 4		0.2100	
Bolts		0.0740	
		Total: 0.7025	
Support	853000		fw1
Primary flywheel		1.8	
Secondary flywheel	Non-linear	0.9	fw2

3.1 Rig modelling

In measurements a resonance around 15 Hz was observed, involving mainly the DMF. There also appear to be resonances of higher frequencies that depend on propeller shaft joint angles. A good model of the rig contributes to the understanding of the measured vibrations and simplifies evaluation.

For steady-state conditions and linear rig properties, the displacements at different positions in the rig can be estimated based on the measured torque τ_{tm} and the measured angular velocity at the primary flywheel $\dot{\varphi}_{fw1}$ as follows.

A lumped mass system of the rig can be formed according to figure 4. Here τ denotes torque and φ angular displacement. How the different parts have been lumped is shown in table 3. For steady-state solutions, the
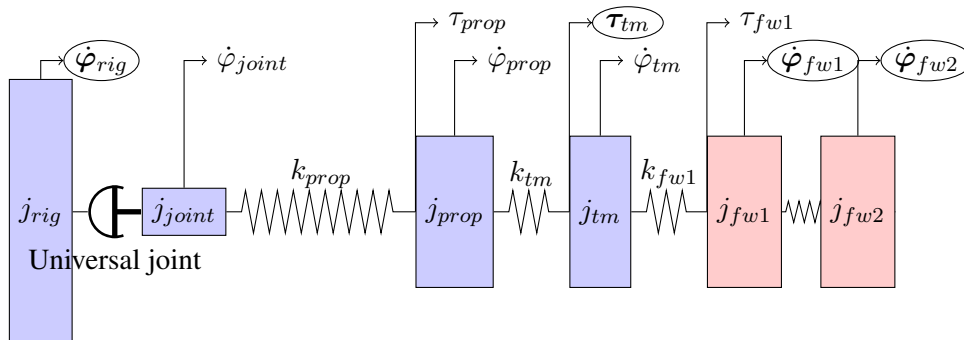

Figure 4: Schematic picture of the rig (encircled variables are measured)

different variables can be estimated as complex series according to equation (2).

$$\varphi_{tm} = \sum_{q=-n}^{n} A_q e^{iq\omega t}, \ \varphi_{fw} = \sum_{q=-n}^{n} B_q e^{iq\omega t}, \ \tau_{tm} = \sum_{q=-n}^{n} T_q e^{iq\omega t} \tag{2}$$

Here A_q, B_q and T_q are complex constants, t is the time and ω is the average angular velocity. The integer n is selected in order to estimate the measured signals with good accuracy. In this work, a value of 8 has been used. The angular velocities and accelerations can also be expressed accordingly. From angular momentum balance, we obtain

$$
\begin{aligned}
j_{tm}\ddot{\varphi}_{tm} &= \tau_{tm} + k_{fw1}(\varphi_{fw1} - \varphi_{tm}) \\
\Rightarrow j_{tm}\ddot{\varphi}_{tm} + k_{fw1}\varphi_{tm} &= \tau_{tm} + k_{fw1}\varphi_{fw1}
\end{aligned}
\tag{3}
$$

Inserting the expressions from (2) into (3) gives

$$
\sum_{q=-n}^{n} \left(-\omega^2 q^2 j_{tm}A_q + k_{fw1}A_q\right) e^{iq\omega t} = \sum_{q=-n}^{n} \left(T_q + k_{fw1}B_q\right) e^{iq\omega t}
\tag{4}
$$

Due to the orthogonality of the functions $e^{iq\omega t}$ we have for all q that

$$
A_q = \frac{T_q + k_{fw1}B_q}{-\omega^2 q^2 j_{tm} + k_{fw1}}.
\tag{5}
$$

Once φ_{tm} is calculated, φ_{prop} can be obtained from equation (6).

$$
\varphi_{prop} = \frac{\tau_{tm} + k_{tm}\varphi_{tm}}{k_{tm}}
\tag{6}
$$

The displacement, on the DMF side of the universal joint, φ_{joint} is then given by equation (7).

$$
\varphi_{joint} = \frac{j_{prop}\ddot{\varphi}_{prop} + \tau_{tm} + k_{prop}\varphi_{prop}}{k_{prop}}
\tag{7}
$$

Based on this, τ_{prop} can be calculated according to equation (8).

$$
\tau_{prop} = -k_{prop}(\varphi_{prop} - \varphi_{joint})
\tag{8}
$$

The equations presented here are based on linear stiffness and no damping. It should be noted, that for higher orders, a correct timing between the signals and very accurate stiffness in the model are of extreme importance. Small deviations in timing can introduce unrealistically high oscillations for higher orders.

4 Simulations

4.1 Computational method

Due to the big number of gap activated springs in the model, conventional time integration methods require very small time steps in order to converge. In the correlation work, a method inspired by [8] has been used. The algorithm first solves a linear complementary problem, assuming that the friction forces are the same as the previous time step and then iterates in order to solve for the updated friction forces. The steady-state harmonic response of a linearised model has been used to impose realistic initial conditions. The simulations have been run until steady-state and the last two cycles have been used for evaluation.

4.2 System modelling

There are several alternatives for the engineering model used in simulation that can be considered in correlation work. The simplest approach is to include only the DMF in the model and impose the measured angular velocities at the primary flywheel in the simulation. Another alternative is to include all parts between torque meter and DMF and apply the measured torque in the simulation. The drawback with these alternatives is that resonance frequencies in the models differ from the full rig system.

A third alternative is to include the rig in the model. The universal joint in the propeller shaft imposes some problems, though. Besides difficulties with implementation and increased simulation time, there are some uncertainties regarding internal clearance, joint angle and joint angular position. A simplification is to model the rig system from the propeller shaft joint to the DMF and apply φ_{joint}, as derived in section 3.1, as a boundary condition.

In figure 5 the relative displacement amplitudes between the primary and secondary flywheel in the DMF are shown for the second vibration order for different propeller shaft joint angles and different rotational speeds. Measured results are shown as solid lines. Simulated results, using only the DMF in the model, are shown as dashed lines. We see that the correlation is not as good for speeds below 500 rpm as for the higher speeds.
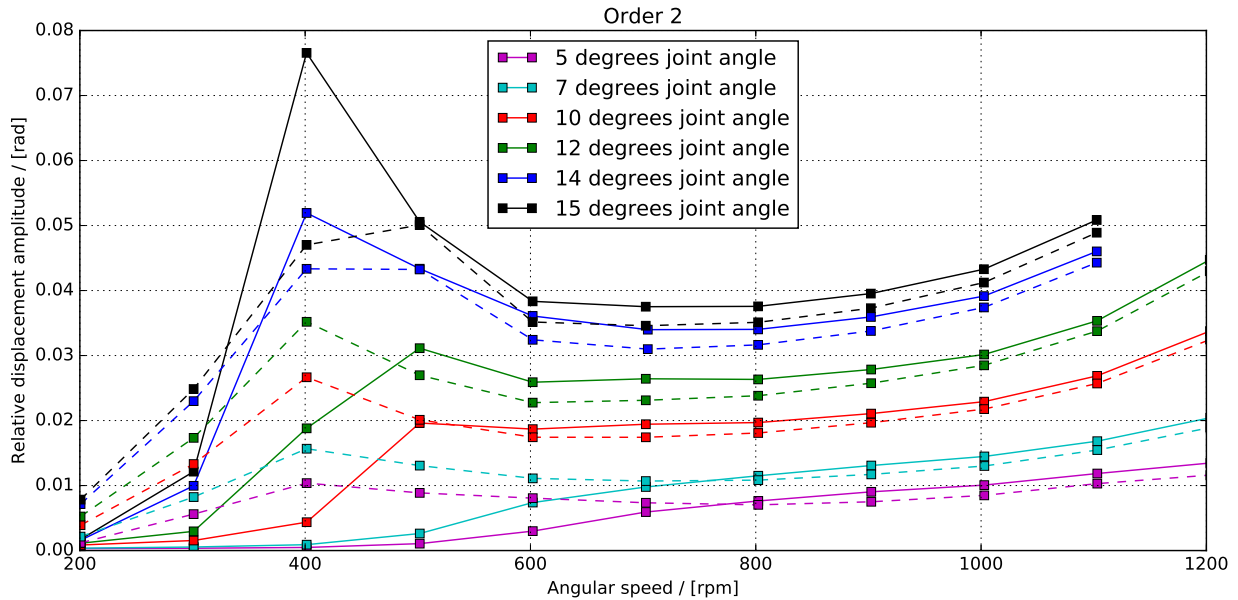

Figure 5: Measured (solid lines) and simulated (dashed lines) relative displacement amplitudes between primary and secondary flywheel

In particular, there is a clear resonance peak in the measurements with 14 and 15 degrees joint angle at 400 rpm that is not captured very well in the simulations. The resonance peak is only visible for the two highest propeller shaft joint angles. Considering that the stiffness of the DMF is lower for lower deflection angles, resonance peaks for lower joint angles can be expected at lower speeds. This is not what is observed in the measurements.

The explanation to this is probably the non-linearities in the rig propeller shaft. As shown in section 3.1, the displacement φ_{prop} at the propeller shaft end closest to the DMF can be estimated from the measured signals τ_{tm} and $\dot{\varphi}_{fw1}$. If the angular position of the universal joint relative the rig flywheel is known, the velocity just after the joint (assuming a stiff joint), can be calculated based on the joint angle and the measured rig flywheel velocity, $\dot{\varphi}_{rig}$. If calculated this way, it will be labelled $\hat{\dot{\varphi}}_{joint}$. The relative displacement in the propeller shaft can then be estimated as

$$\Delta_{prop} = \varphi_{prop} - \hat{\varphi}_{joint} \tag{9}$$

In this work, the angular position of the rig flywheel could be determined thanks to small deviations in the rig timing gear geometry. These deviations caused reoccurring spikes in the measured signal that were used to determine the position. How the universal joint is rotated relative the rig flywheel determines the phase of the angular velocity oscillation after the joint. By inspecting the angular velocity after the joint, $\dot{\varphi}_{joint}$, as derived in section 3.1, the angular position of the universal joint relative the rig flywheel could be estimated.

Figure 6 shows the relationship between the estimated second order of the torque at the end of the propeller shaft τ_{prop} as a function of the second order of the estimated propeller shaft deflection, Δ_{prop}. The squares denote speeds below 700 rpm and the dashed line shows the propeller shaft stiffness calculated from the geometry. As can be seen we have a fairly linear relationship for speeds at 700 rpm and higher. The curve
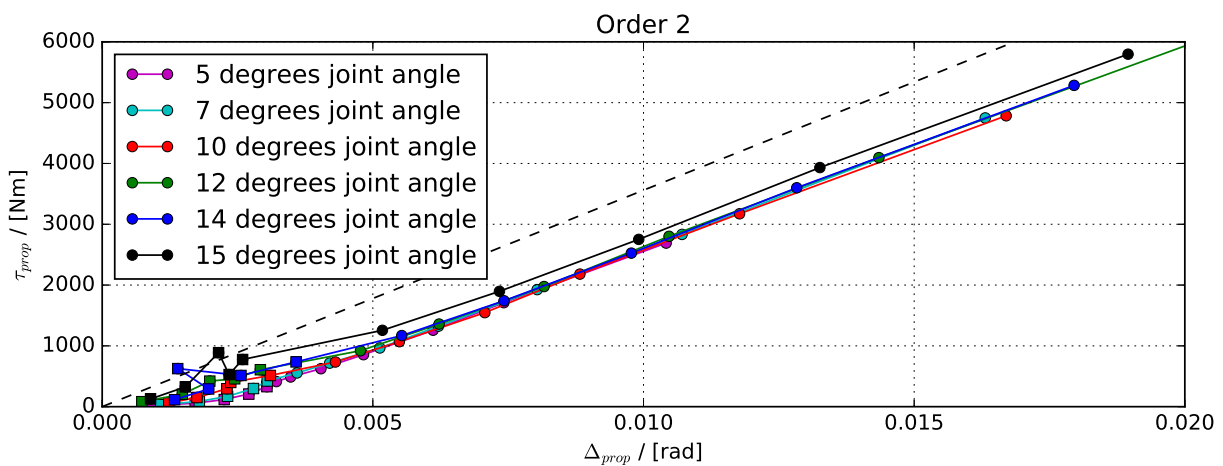

Figure 6: Propeller shaft stiffness

follows the expected stiffness of the propeller shaft well, but with an offset. This indicates that there is an internal clearance and a very non-linear stiffness in the propeller shaft joint for small deflection angles. At small deflection angles, the resonance behaviour is governed both by high non-linearities in the DMF and in the propeller shaft joint.

Several different rig modelling approaches have been used and compared, in order to capture the resonances in a better way. Improvement for some joint angles lead to worse results for other angles. Apart from near resonances, there are small differences in the results from the different approaches.

Since the focus of this work is the DMF model and not the rig it was decided to concentrate on correlation for speeds above the resonance. Results for the lowest propeller shaft joint angles were also omitted in the correlation work, since those results are extremely sensitive to the internal clearances in the DMF. Additional measurements are needed in order to model these non-linearities in an accurate way.

In section 5, the simulated results are based on the model including only the DMF and with measured angular velocities as boundary conditions for the primary flywheel.

5   Correlation

In figure 7, the relative angular displacement between the primary and secondary flywheel is shown for measurements and simulations. Far from resonance, the friction and damping parameters have relatively small influence on the relative displacement, so the good correlation is not surprising. In order to better assess the
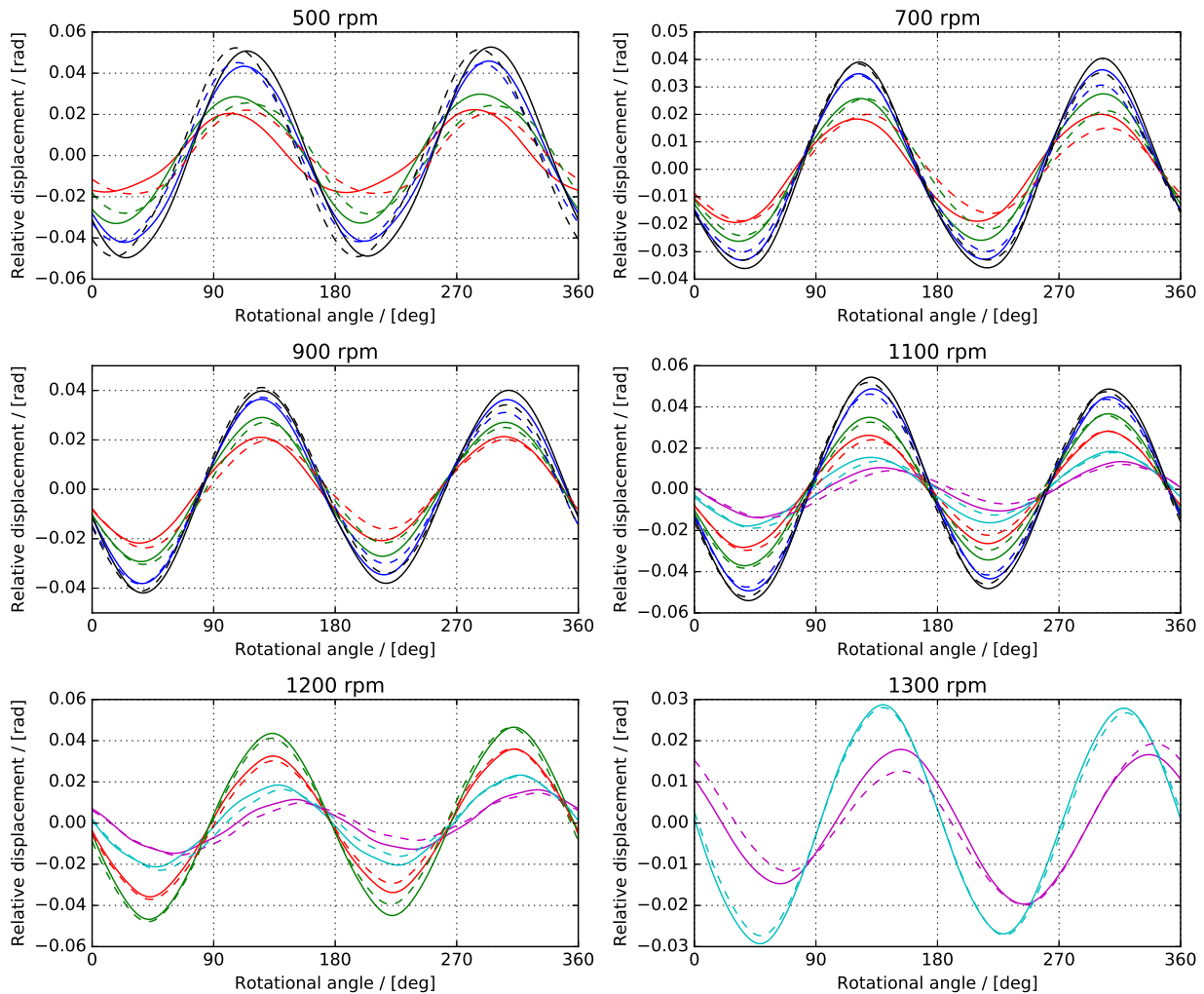

Figure 7: Relative angular displacement between secondary and primary flywheel for different speeds from measurements (solid lines) and simulations (dashed lines). Colours denote joint angles as in figure 5.

validity of the friction model the hysteresis curves are analysed. In figure 8, the torque into the secondary flywheel is shown as a function of the relative displacement between the two flywheels. Only orders up to 12 are included in order to filter out noise and high-frequency vibrations. It should be noted that small measurement errors in the angular velocity of the secondary flywheel can have a significant impact on the higher orders of the calculated torque. It has been difficult to determine if the deviations between measurements and simulations that exist are due mainly to the modelling or to the resolution in the measurements.

Even though the measured results are not exactly reproduced, the general behaviour of the DMF is captured. We can see clear trends of higher energy dissipation per cycle at higher speeds and also higher effective stiffness. At higher speeds the sliding shoes do not move in a uniform manner, which explains the non-linear variation of the torque.

The effect of the Coulomb coefficient of friction is illustrated in figure 9a for the case with rotational speed of 800 rpm and 15 degrees propeller shaft joint angle. Simulated results are shown with coefficients of friction
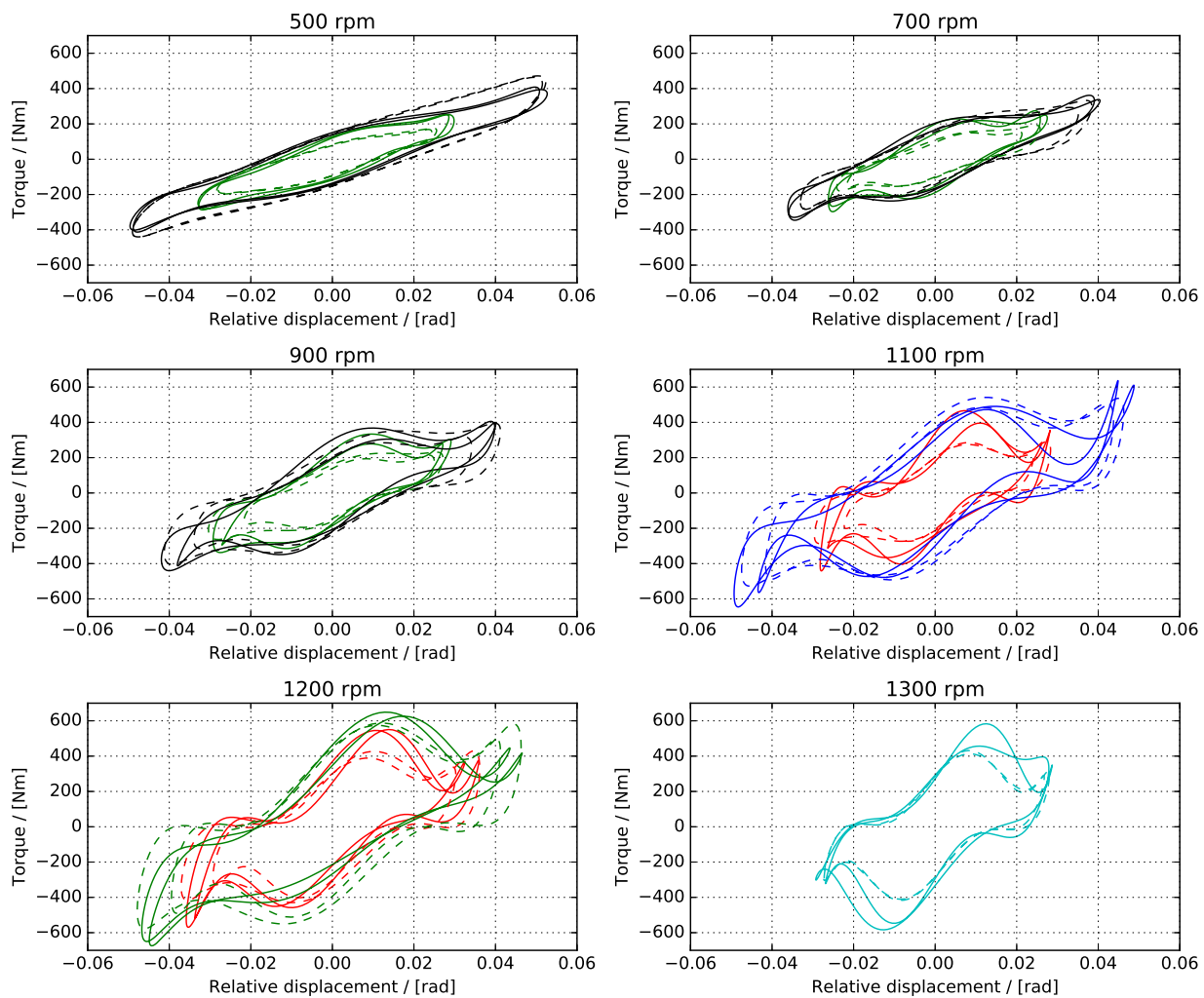
Figure 8: Torque-displacement relationship at different speeds from measurements (solid lines) and simulations (dashed lines). Colours denote joint angles as in figure 5.

of zero and 0.08. The difference is quite small and the reason is the low normal force. For higher mean torques the coefficient of friction is expected to affect the results in a more significant way.

In the measurements there is generally a steep increase in torque at secondary flywheel for small relative displacements. This indicates that there is significant viscous damping, since this is where the relative velocities between the sliding shoes and the primary flywheel are high. In figure 9b simulated results without the viscous part in the friction model are shown for two different coefficients of friction. We can note much lower torque magnitudes at small relative displacements than in corresponding results from the measurements. The impact of the different friction parameters is similar at higher speeds.

6   Conclusions

The proposed model of the DMF has shown to produce realistic results for a big range of speeds and load amplitudes. The results indicate that there is a significant amount of viscous damping between the sliding shoes and primary flywheel. This must be included in the friction modelling and considering only Coulomb friction does not produce satisfactory results. The effect of the Coulomb friction in the analysed model is quite small compared to the viscous part, but it is expected to be more important for higher average torque and higher rotational speeds.

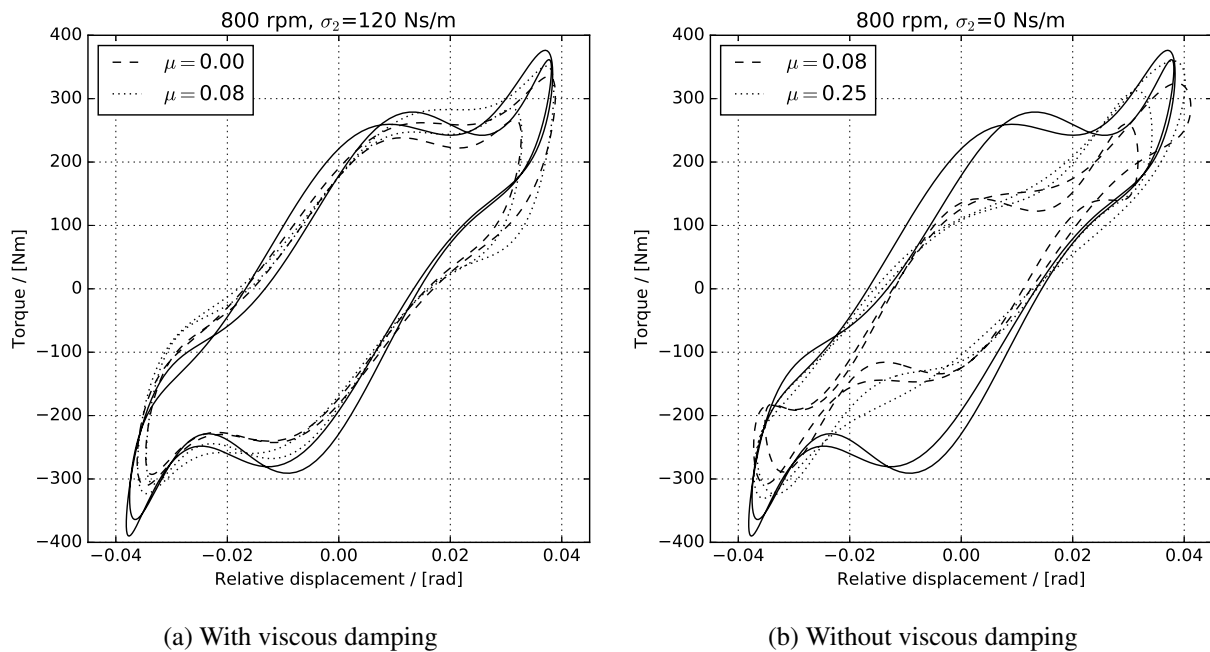(a) With viscous damping

(b) Without viscous damping

Figure 9: Torque-displacement relationship from measurements (solid lines) and simulations (dashed and dotted lines) with different parameter settings

There are several resonances in the analysed system and accurate modelling of the internal gaps and spring stiffnesses is very important to capture the oscillating behaviour of the systems near these resonances. Correlation could be improved further with accurate measurements of the internal clearances. However, for higher mean torques which corresponds to normal operating conditions, the impact of internal clearances is not as big.

Future work will focus on the validity of the model for higher mean torques at different load amplitudes and frequencies.

Acknowledgements

References

[1]   A. Albers et al. "New Methodology for Power Train Development in the Automotive Engineering - Integration of Simulation, Design and Testing". In: *SAE Technical Papers*. 2001.

[2]   J. Karlsson. *Investigation of dynamic friction properties of a dual mass flywheel for commercial vehicles*. M. Sc. thesis. Chalmers University of Technology. 2018.

[3]   P. Kelly et al. "Dual mass flywheel as a means of attenuating rattle". In: *Tribology and Dynamics of Engine and Powertrain* (2010), pp. 857–877.

[4]   T. H. Kim et al. "Analysis of Dual Mass Flywheel Using Discrete Arcspring Model". In: *Key Engineering Materials* 326-328 (2006), pp. 1607–1610. ISSN: 1662-9795.

[5]   T. Mahl and O. Sawodny. "Modelling of an automotive Dual Mass Flywheel". In: *IFAC Proceedings Volumes (IFAC-PapersOnline)*. Vol. 43. 18. IFAC, 2010, pp. 517–523. ISBN: 9783902661760.

[6]   H. Olsson. "Control Systems with Friction". PhD thesis. Lund Institute of Technology, 1996. ISBN: 0280-5316.

[7]   U. Schaper et al. "Modeling and torque estimation of an automotive dual mass flywheel". In: *Proceedings of the American Control Conference*. 2009, pp. 1207–1212. ISBN: 9781424445240.

[8]   S. D. Yu. "An efficient computational method for vibration analysis of unsymmetric piecewise-linear dynamical systems with multiple degrees of freedom". In: *Nonlinear Dynamics* 71.3 (2013), pp. 493–504. ISSN: 0924090X.